

Investigations of the electronic and optical properties of $V_2\text{InC}$ and $V_2\text{InN}$ based MAX phases in the framework of density functional theory

Bakhtiar Ul Haq^{a,b,*}, Se-Hun Kim^{a,**}, S. AlFaify^b, S.A. Tahir^c, R. Ahmed^{c,d}, Samah Al-Qaisi^e, A. Laref^f

^a Faculty of Science Education, Jeju National University, Jeju, 63243, Republic of Korea

^b Department of Physics, Faculty of Science, King Khalid University, P.O. Box 9004, Abha, Saudi Arabia

^c Center for High Energy Physics, University of the Punjab, Quaid-e-Azam Campus, Lahore, 54590, Pakistan

^d Department of Physics, Faculty of Science, Universiti Teknologi Malaysia, UTM, Skudai, 81310, Johor, Malaysia

^e Palestinian Ministry of Education and Higher Education, Nablus, Palestine

^f Department of Physics and Astronomy, College of Science, King Saud University, Riyadh, 11451, Saudi Arabia

ARTICLE INFO

Communicated by Luis Brey

Keywords:

MAX phases
Density functional theory
Electronic structures
Conductivity
Absorption spectra

ABSTRACT

This work reports a new class of MAX phases based on $V_2\text{InC}$ and $V_2\text{InN}$ for advanced technological applications. We use the “density functional theory (DFT)-based full-potential linearized augmented-plane-wave (FP-LAPW) approach” to investigate the lattice constants, electronic, and optical properties of $V_2\text{InC}$ and $V_2\text{InN}$. The lattice constants a (c) of the studied MAX phases have been recorded as 3.01 Å (12.60 Å) for $V_2\text{InC}$ and 3.03 Å (12.40 Å) for $V_2\text{InN}$, which have been found well-matching to the available literature. Like other MAX phases, the studied compounds are metallic, as the valence band’s energy states overlap with those in the conduction band over the Fermi level. The major contribution to the electronic structure is seen from the $V-d$, $\text{In}-s$, p , and $X-p$ states. Similarly, the studied MAX phases show prominent light absorption, enhanced by order 10 in the visible range and 10^2 in the ultraviolet (UV) range of the electromagnetic spectrum. Additionally, the $V_2\text{InC}$ and $V_2\text{InN}$ demonstrated anisotropic optical conductivity, which shows interesting variations with the energy of incident light. The optical conductivity exhibits threshold behavior in the infrared range, significant improvement in the visible range, and the highest conductivity in the ultraviolet range. The information provided in our study will likely be useful for future research on $V_2\text{InC}$ and $V_2\text{InN}$ MAX phases.

1. Introduction

The hexagonal structured ternary carbide/nitride, also known as the MAX phases, has recently received significant interest from researchers. These materials are comprised of transition metals (M), Group-A elements (A), and Carbon/Nitrogen (X) and are denoted by the formula $M_{n+1}AX_n$ ($n = 1, 2, 3$) [1]. The integer n classifies the MAX phases into different phases, such as M_2AX , M_3AX_2 , and M_4AX_3 [2,3]. Moreover, an abundance of the MAX phases strongly depends on the value of n . For instance, the MAX phases with $n = 1$ occur the highest in number. Around sixty MAX phases for $n = 1$ have been synthesized in the experiment, and 150 additional such candidates have been predicted [3–6]. Following $n = 1$, the abundance of MAX phases is followed by $n = 2$ and $n = 3$. Similarly, a few MAX phases for $n = 4$ have also been

reported in the literature [3].

At room temperature and pressure, the MAX phases occur in hexagonal symmetry of the space group No. 194 ($P6_3/mmc$) [7], where a covalent bond connects the transition metals and Carbon/Nitrogen atoms in the form of $M_{n+1}X_n$ octahedron. These edge-shared $M_{n+1}X_n$ octahedral blocks are sandwiched between the atomic layers composed of Group A elements along the z -axis. The MAX phases simultaneously own metallic and ceramic behavior mainly resulting from the more metallic bonding between the transition metals and A atoms and more covalent bonds between transition metals and X atoms [8]. Therefore, they have received renewed interest due to their exciting behavior, such as good electrical and thermal conductivities, resistance to oxidation, low density, excellent thermal shock, and easy machinability [9–11]. Therefore, they have found reliable applications as a substitute for

* Corresponding author. Faculty of Science Education, Jeju National University, Jeju, 63243, Republic of Korea.

** Corresponding author. Faculty of Science Education, Jeju National University, Jeju, 63243, Republic of Korea.

E-mail addresses: bakhtiarjadoon@gmail.com, bakhtiar@jejunu.ac.kr (B. Ul Haq), spinji@jejunu.ac.kr (S.-H. Kim).

graphite, particularly for applications requiring high temperatures, sensors, high-temperature ceramics, tribological components, electrical contacts for catalysis, gas burner nozzles, protective coatings, concrete's dry drilling, etc., [1–7,9–20]. Due to these exciting applications, MAX phase materials have been the subject of numerous experimental and first principles studies recently [1–7,9–22].

A recent study reported the physical properties, including thermodynamic, elastic, and thermoelectric properties of M_2AC and M_2AB ($M = Nb$ or Mo and $A = Al$ or Ga), where Mo_2AlC , in particular, showed distinct characteristics, including a higher cohesive energy and interesting thermoelectric behavior [23]. Furthermore, the fabrication of magnetic MAX phases in recent years has furthered applications of the MAX phases to the field of spintronics [24–26]. These studies show that the MAX phases' physical properties strongly depend on the constituent atoms' selection. Accordingly, the vanadium-based MAX phases have been studied and reported to demonstrate attractive elastic, transport, and electronic properties [27,28]. Furthermore, as an attractive electronic behavior owner, the V-based MAX phases are expected to demonstrate interesting optical properties. However, the electronic properties of the V-based MAX phases have been scarcely studied to date.

This article reports the optical properties of V-based MAX phases, such as V_2InC and V_2InN , using the effective “FP-LAPW approach in DFT.” In addition to the optical properties, we comprehensively studied their structural and electronic properties. Our study will likely provide a deep insight into the electronic and optical behavior of this new class of V-based MAX phases for futuristic theoretical and experimental studies.

2. Computational details

The “FP-LAPW approach framed within DFT” was utilized to carry out the calculations of the physical properties of the V_2InC and V_2InN MAX phases. This method accurately depicts the electronic structure compared to alternative approaches. We employed the WIEN2k code [29] to perform these calculations, a highly regarded and extensively utilized software package renowned for its comprehensive suite of tools designed for electronic structure calculations. The Generalized Gradient Approximation (GGA) was employed to estimate the exchange and correlation effects of the electrons. To accomplish this, the Perdew-Burke-Ernzerhof (PBE) [30] parameterization of the GGA was employed, demonstrating its reliability in producing accurate results [31–44]. The muffin tin radius (R_{MT}) spheres were utilized in atomic units (a.u) with the following values:

$V = 2.02$ a.u, $In = 2.50$ a.u, and $C = 1.65$ a.u in the case of V_2InC .

$V = 1.94$ a.u, $In = 2.50$ a.u, and $N = 1.67$ a.u in the case of V_2InN .

In order to ensure an accurate sampling of the Brillouin zone, a k -mesh grid of dimensions $12 \times 12 \times 1$ was utilized. This higher density of k -points enables a more precise characterization of electronic properties. The wave functions were expanded using plane waves, incorporating angular momentum quantum numbers up to a maximum value of $l_{max} = 10$. By controlling this expansion parameter, the wave-function expansion encompasses the most significant angular momentum components, leading to an adequate representation of the electronic wave functions. The electron distribution within the crystal was limited in reciprocal space by employing a cutoff parameter of $G_{max} = 16 \text{ au}^{-1}$, thereby characterizing the charge density. To determine the energy cutoff, denoted as K_{max} , $K_{max} = 8.0/R_{MT} (\text{Ry})^{1/2}$ was utilized. A convergence criterion of 10^{-5} Ry per unit cell was established for the total energy.

3. Results and discussion

The V_2InC and V_2InN compounds of the 211-MAX phases form in

wurtzite structures of space group No 194 ($P6_3/mmc$). The unit cells of the V_2InC and V_2InN atoms comprise two formula units at $(1/3, 2/3, z)$ Wyckoff position. Similarly, the In atom fills the $(1/3, 2/3, 3/4)$ Wyckoff position, whereas the X atoms are stationed at the $(0, 0, 0)$ site. Fig. 1 shows that Vn, In, and X atoms are arranged in the vertically stacked atomic layers along the c -direction. Each X atom is bonded with six V atoms, forming a V_6X octahedron. These V_6X are surrounded by In layers from both sides along the c -axis. These 211-MAX phases exhibit symmetrical a and b lattice constants recorded as 2.90 \AA for V_2InC and 2.91 \AA for V_2InN . The calculated lattice constant (a) is comparable to that reported for V_2InC and V_2InN as 3.00 \AA [45], 2.969 \AA [46], and 2.966 \AA [45], respectively. The V_2InC and V_2InN compounds exhibited the c -lattice constant as 12.60 \AA and 12.40 \AA , respectively. These results for lattice constant ' c ' are excellently comparable to that reported as 13.491 \AA [45] and 13.326 \AA [46] for V_2InC and 13.574 \AA [45] for V_2InN .

We then calculated the cohesive energies (E_{coh}) for V_2InC and V_2InN compounds to realize their energetic stability. The E_{coh} , which is the difference between the energy of the V_2InC and V_2InN compounds ($E_{V_2GaX}^{211-MAX}$) and their constituents ($E_V + E_{In} + E_{C,N}$), are being calculated using Eq. (1)

$$E_{coh} = (E_{V_2GaX}^{211-MAX}) - (xE_V + yE_{In} + zE_{C,N}) / (x + y + z) \quad (1)$$

The E_{coh} for V_2InC and V_2InN compounds has been recorded as -5.95 eV and -5.51 eV , respectively, for V_2InC and V_2InN , which is in good agreement with 6.29 eV [47] reported for Ti_2AlC , 4.40 eV for Y_2AlB [48], 6.09 eV for Ti_2AlN [47], 7.183 eV for Ti_2CdC [49], and 5.20 eV for Sc_2AlB [48].

Fig. 2 provides the band structures of V_2InC and V_2InN compounds determined along the Γ -M-K- Γ -A path in the Brillouin zone. One can see from Fig. 2 that valence band states have been extended to the conduction band over the Fermi level. The overlapping of valence and conduction bands over the Fermi level leaves the V_2InC and V_2InN

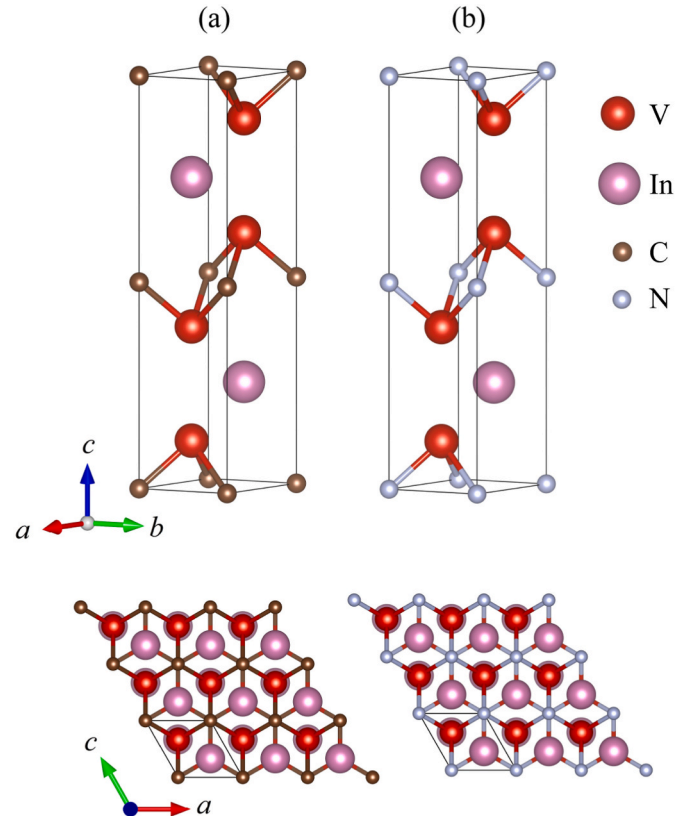


Fig. 1. The crystal structure of (a) V_2InC and (b) V_2InN depicted in different orientations.

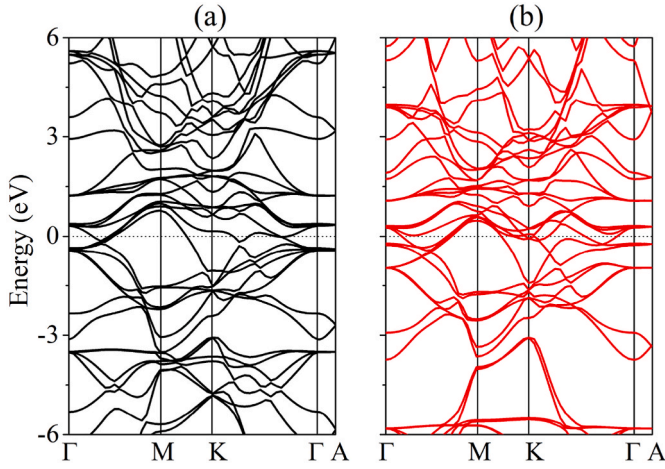


Fig. 2. The electronic structures of (a) V_2InC and (b) V_2InN determined against energy.

compounds as metallic materials due to the lack of an apparent band gap. This is expected as the intrinsic MAX phases are metallic. Fig. 3, showing the DOS, indicates the existence of considerable states over the Fermi level. The states appearing over the Fermi level are mainly derived from the V-d states. The V-d states appear with substantial density in the vicinity of the Fermi level in the case of all three compounds. However, a considerable contribution to the electronic structures can also be seen from the In-p and X-p states in the lower conduction and upper valence bands.

To investigate the optical properties of V_2InC and V_2InN , calculations

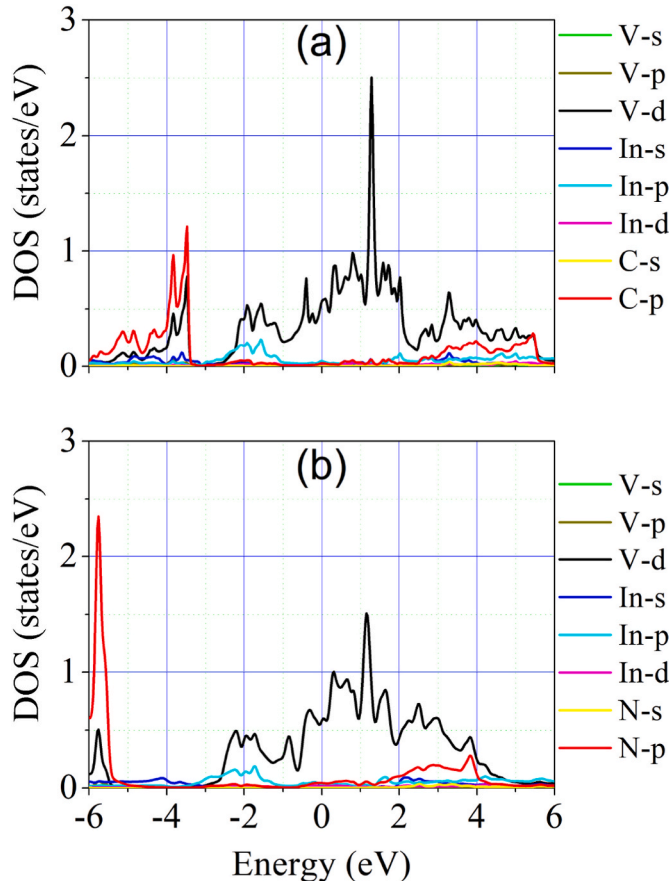


Fig. 3. The DOS of (a) V_2InC and (b) V_2InN determined against energy.

for the dielectric function (real ($\epsilon_1(\omega)$) and imaginary ($\epsilon_2(\omega)$) components) displayed in Fig. 4 were performed using the following Eqs. (1) and (2).

$$\epsilon_1(\omega) = 1 + \frac{2}{\pi} P \int_0^\infty \frac{\omega' \epsilon_2(\omega')}{\omega'^2 - \omega^2} d\omega' \quad (1)$$

$$\epsilon_2(\omega) = \frac{2e^2\pi}{\Omega \epsilon_0} \sum_{k,V,C} |\Psi_k^C[\vec{u},\vec{r}] \Psi_k^C|^2 \delta(E_k^C - E_k^V - E) \quad (2)$$

As seen in Fig. 4 (a, b), the main peak in the $\epsilon_1(\omega)$ dispersion occurs in the electromagnetic spectrum's infrared region. The V_2InC and V_2InN exhibit a significant degree of anisotropy in the $\epsilon_1(\omega)$ dispersion. The x-component of static dielectric constants ($\epsilon_1(0)$) for V_2InC and V_2InN displays values of 70.28 and 81.51 respectively. On the other hand, for V_2InC and V_2InN , the z-component of $\epsilon_1(0)$ has been estimated to be 93.76 and 116.23, respectively. While proceeding into the ultraviolet spectrum, the $\epsilon_1(\omega)$ dispersion shows a sharp decline, and in certain electromagnetic spectrum ranges, it even takes negative values associated with the metallic behavior of V_2InC and V_2InN . Fig. 4(c and d) illustrates that peaks in $\epsilon_2(\omega)$ is governed by electronic transitions from lower energy levels to higher ones. Due to the metallic nature of MAX phases, these electronic transitions can occur even at very low energy levels. Consequently, a prominent peak is observed in the $\epsilon_2(\omega)$ spectrum at low photon energies. Notably, the amplitude of the x-component of $\epsilon_2(\omega)$ is significantly larger than that of the z-component, and the z-component's maximum amplitude occurs at a higher energy level compared to the x-component. The difference in amplitudes can be attributed to the energy absorbed by electrons during their transition from lower to higher energy levels induced by incident light. This suggests that V_2InC and V_2InN MAX phases, therefore, display distinct optical properties along the x- and z-directions that are discussed in the following.

The refraction and reflection of light by these V_2InC and V_2InN compounds have been schematically shown in Figs. 5 and 6. The optical refraction by V_2InC and V_2InN compounds has been found to be the highest for infrared light. The static refractive indices have been seen as 8.42 (9.85 z-component) and 9.05 (10.81 z-component) for V_2InC and V_2InN respectively. However, the refractive indices are found to be declined dramatically for visible and ultraviolet light. This indicates that while the V_2InC and V_2InN compounds can efficiently refract infrared light, visible and UV light refraction is considerably reduced, indicating the transition to opaque from transparent nature. However, Fig. 6 still shows the refractive indices remain higher than unity for the light photons of energy less than 10 eV. Figs. 5 and 6 reveal that a decline in the refractive indices is followed by a reduction in the optical reflection. Like optical refraction, the reflection of infrared light has been found to be the highest for the V_2InC and V_2InN compounds and goes through a rapid decline for UV and visible radiation. The V_2InC and V_2InN compounds could reflect more than 50 % of the incident light, more than 40 % of visible light, and UV radiations (of energy <10 eV). The optical reflection diminishes radiation of energy above 20 eV. The high optical reflectivity is due to the metallic nature of the V_2InC and V_2InN compounds.

While V_2InC and V_2InN refract or reflect some of the incident radiation, the charge carriers absorb the rest of the light to hop to high energy states. In Fig. 7, the absorption of infrared light is considerable, indicating that even low-energy photons can trigger the intra-band transitions within the electronic structures of these compounds. This is because they exhibit gapless electronic structures; therefore, the transition between low and high-energy photons can be successfully executed by low-energy photons. However, these electronic transitions are rapidly enhanced as the relatively high-energy photons interact with these materials. As a result, the optical spectra' amplitude has been significantly improved in the visible and UV range. The optical absorption in the infrared, visible, and UV ranges have been found of the

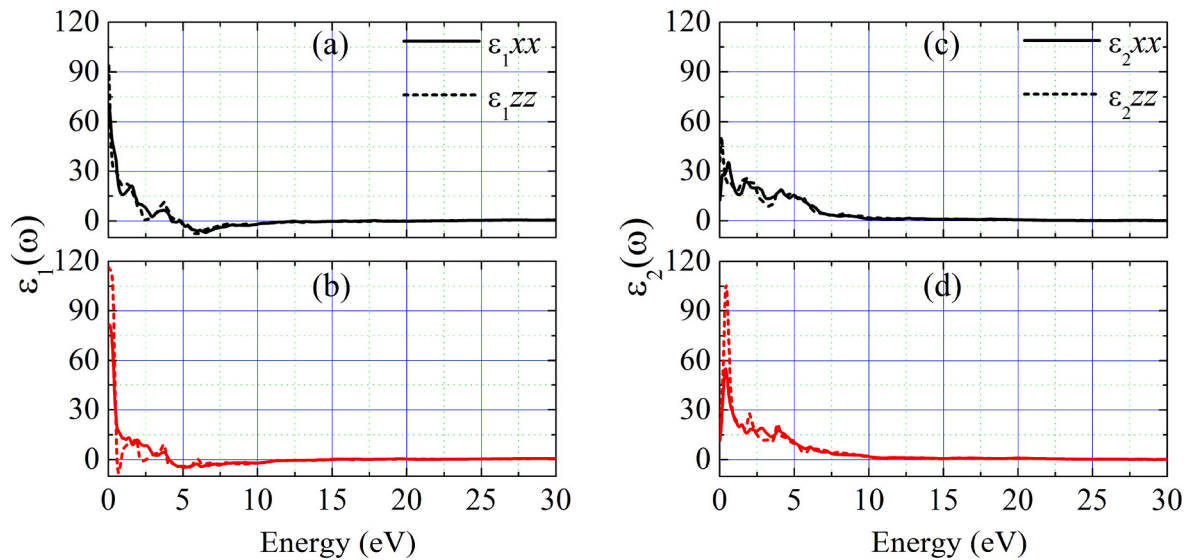


Fig. 4. The $\epsilon_1(\omega)$ of V_2InC (a) and V_2InN (b) and $\epsilon_2(\omega)$ of V_2InC (c) and V_2InN (d) determined against the energy.

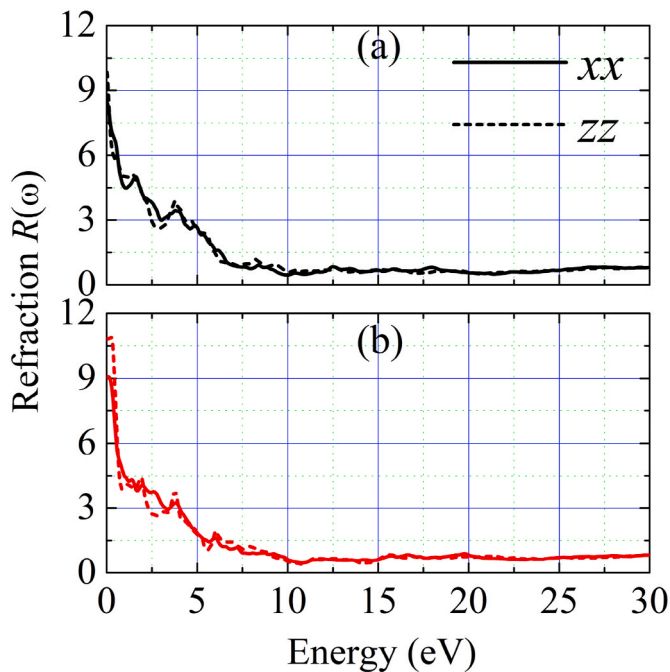


Fig. 5. The optical refraction spectrum of (a) V_2InC and (b) V_2InN determined against the energy of the incident light photons.

order 10^4 cm^{-1} , 10^5 cm^{-1} , and 10^6 cm^{-1} , respectively. This indicates that optical absorption is enhanced by order 10 in the visible range and 10^2 in the UV range of the electromagnetic spectrum. Such a high capacity of light absorption indicates the capability of the V_2InC and V_2InN compounds in high-efficiency energy harvesting devices.

Fig. 8 depicts the optical conductivity of V_2InC and V_2InN against the energy of light photons. Optical conductivity is a material's capacity to conduct electricity while being exposed to light. When light interacts with a material, the incident light photons excite electrons, causing them to move from low to high energy levels and create an electric current. The V_2InC and V_2InN showed the threshold optical conductivity when exposed to infrared light because of their metallic behaviour. V_2InC and V_2InN exhibit a significant increase in optical conductivity as photon energy rises and enters the visible light region. With this

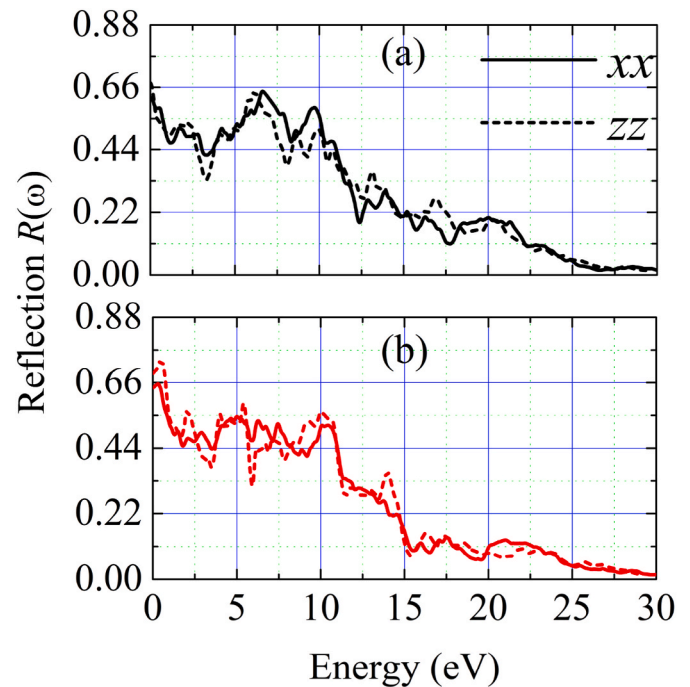


Fig. 6. The reflectivity spectrum of (a) V_2InC and (b) V_2InN determined against the energy of the incident light photons.

development, the material will conduct electricity when exposed to visible light significantly more effectively. In the energy range of 4 eV–6 eV, the V_2InC and V_2InN show their highest optical conductivity, suggesting that these materials exhibit excellent electrical conduction properties when interacting with ultraviolet light.

The optical conductivity of V_2InC and V_2InN displays anisotropy in the x- and z-directions. This indicates that depending on the direction of the incident light with regard to the crystal structure of V_2InC and V_2InN , its optical conductivity can change. The maximum optical conductivity is shown in V_2InC when compared to V_2InN . This shows that when exposed to light, V_2InC is the most effective at conducting electricity, followed by V_2InN . The difference in their conductive properties can be attributed to their specific electronic band structures and chemical compositions. However, as the photon energy goes even higher

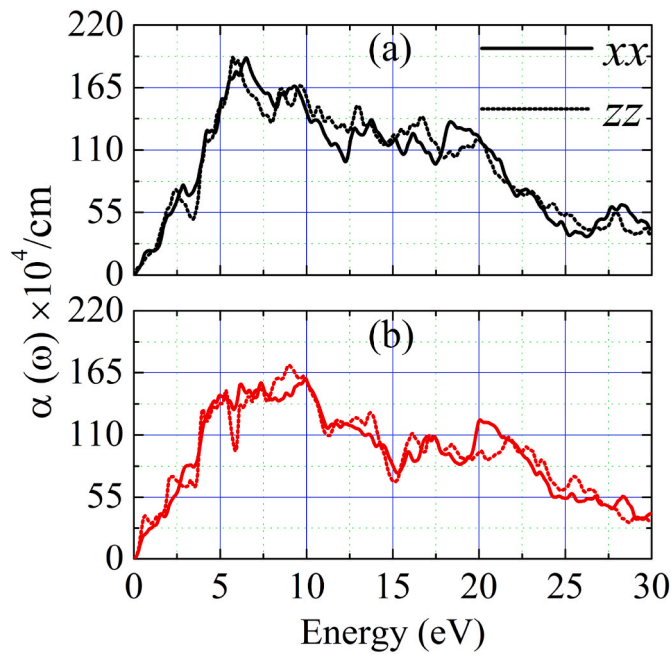


Fig. 7. The optical absorption spectrum of (a) V_2InC and (b) V_2InN determined against the energy of the incident light photons.

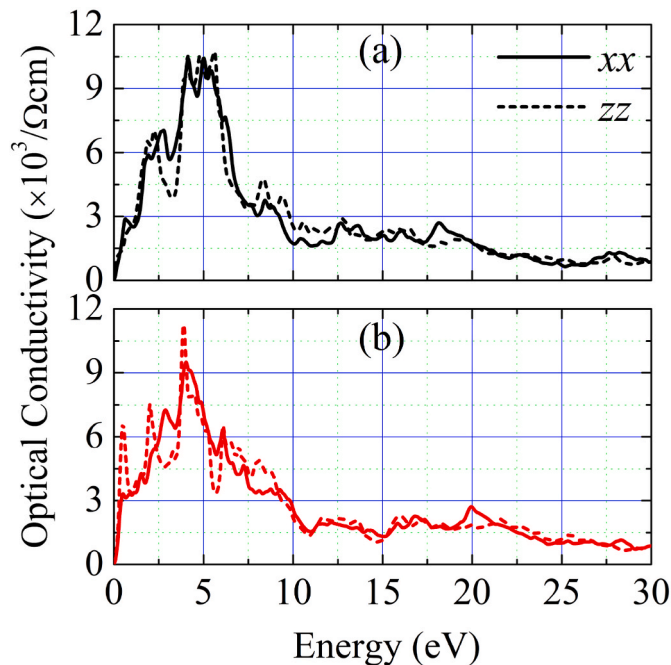


Fig. 8. The optical conductivity of (a) V_2InC and (b) V_2InN determined against the energy of the incident light photons.

beyond this range beyond 6 eV, the optical conductivity of the material starts to reduce. The observed reduction in the optical conductivity can be explained by various physical phenomena such as;

Increased Scattering: Higher-energy photons increase the probability of scattering events, which hinder the effective transport of electrons to the conduction band and can lower the V_2InC and V_2InN compound's overall conductivity.

Saturation of Excited Carriers: Many electrons may have already been stimulated to higher energy states at high photon energies. As a result, the density of excited carriers (electrons in the conduction band)

saturation, which limits the rise in optical conductivity by preventing additional high-energy photons from producing a corresponding increase in the number of excited carriers.

4. Conclusion

In conclusion, this study unveils a new class of MAX phases based on V_2InC and V_2InN with potential applications in advanced technologies. By employing the "DFT-based FP-LAPW approach", we thoroughly investigated the lattice constants, electronic and magnetic behavior, and optical properties of these MAX phases. The obtained lattice constants as 3.015 Å for V_2InC and 3.03 Å for V_2InN , matched well with existing literature. Similar to other MAX phases, the compounds under scrutiny exhibited metallic behavior, characterized by the overlapping of energy states from the valence and conduction bands near the Fermi level. The V-d, In-s, p, and X-p states were found to play a significant role in determining the electronic structure. Additionally, the studied MAX phases demonstrated notable light absorption, optical reflectivity, and refraction. The optical conductivity of V_2InC and V_2InN showed interesting variations with the energy of incident light. It exhibited threshold behavior in the infrared, significant improvement in the visible range, the highest conductivity in the ultraviolet range, and reduced conductivity for high-energy photons. Additionally, these materials displayed anisotropy in conductivity, meaning its conductivity is directionally dependent. The ranking among different V_2InC and V_2InN compositions in terms of optical conductivity is $V_2InC > V_2InN$. Our study provides valuable insights into the physical characteristics of the investigated MAX phases, offering useful information for future research based on these materials.

Author statement

We state that all the authors contributed equally and significantly to this manuscript.

Declaration of competing interest

All the author(s) declare that.

- This has not been published previously.
- It is not under consideration for publication elsewhere.
- Its publication is approved by all authors.
- If accepted, it will not be published elsewhere in the same form, in English or in any other language, including electronically without the written consent of the copyright-holder.

The authors further declare that they have no known competing financial interests or personal relationships that could have appeared to influence the work reported in this paper.

Data availability

Data will be made available on request.

Acknowledgment

This work is supported by the Brain Pool program (No. 2022H1D3A2A02063677) and "Regional Innovation Strategy (RIS)" (No. 2023RIS-009) through the National Research Foundation of Korea (NRF).

References

- [1] M. Ali, M. Hadi, M. Hossain, S. Naqib, A. Islam, Theoretical investigation of structural, elastic, and electronic properties of ternary boride $MoAlB$, *Phys. Status Solidi* 254 (7) (2017), 1700010.

- [2] M. Hadi, Superconducting phases in a remarkable class of metallic ceramics, *J. Phys. Chem. Solid.* 138 (2020), 109275.
- [3] M.A. Rahman, I. Kholil, R. Khatun, S. Sarker, M. Hasan, M.A. Ali, M.Z. Rahaman, K. M. Hossain, M.I. Haque, M.Z. Hasan, High pressure study of new type of MAX phases: Hf_2AB_2 (A = In, Sn), *Phys. Status Solidi (b)* (2022).
- [4] P. Eklund, M. Beckers, U. Jansson, H. Högborg, L. Hultman, The Mn+1AX_n phases: materials science and thin-film processing, *Thin Solid Films* 518 (8) (2010) 1851–1878.
- [5] M. Sokol, V. Natsu, S. Kota, M.W. Barsoum, On the chemical diversity of the MAX phases, *Trends Chem.* 1 (2) (2019) 210–223.
- [6] X. Li, J. Malzbender, G. Yan, J. Gonzalez-Julian, R. Schwaiger, A combined experimental and modeling study revealing the anisotropic mechanical response of Ti_2AlN MAX phase, *J. Eur. Ceram. Soc.* 41 (12) (2021) 5872–5881.
- [7] M.W. Barsoum, T. El-Raghy, The MAX phases: unique new carbide and nitride materials: ternary ceramics turn out to be surprisingly soft and machinable, yet also heat-tolerant, strong and lightweight, *Am. Sci.* 89 (4) (2001) 334–343.
- [8] A. Thore, M. Dahlqvist, B. Alling, J. Rosén, First-principles calculations of the electronic, vibrational, and elastic properties of the magnetic laminate Mn_2GaC , *J. Appl. Phys.* 116 (10) (2014), 103511.
- [9] M.M. Ali, M. Hadi, I. Ahmed, A. Haider, A. Islam, Physical properties of a novel boron-based ternary compound Ti_2InB_2 , *Mater. Today Commun.* 25 (2020), 101600.
- [10] J.-C. Nappé, P. Grosseau, F. Audubert, B. Guilhot, M. Beauvy, M. Benabdellam, I. Monnet, Damages induced by heavy ions in titanium silicon carbide: effects of nuclear and electronic interactions at room temperature, *J. Nucl. Mater.* 385 (2) (2009) 304–307.
- [11] X. Wang, Y. Zhou, Layered machinable and electrically conductive Ti_2AlC and Ti_3AlC_2 ceramics: a review, *J. Mater. Sci. Technol.* 26 (5) (2010) 385–416.
- [12] M.W. Barsoum, MAX Phases: Properties of Machinable Ternary Carbides and Nitrides, John Wiley & Sons, 2013.
- [13] M. Ali, M. Hossain, M. Uddin, A. Islam, D. Jana, S. Naqib, DFT insights into new B-containing 212 MAX phases: Hf_2AB_2 (A = In, Sn), *J. Alloys Compd.* 860 (2021), 158408.
- [14] S. Kota, M. Sokol, M.W. Barsoum, A progress report on the MAB phases: atomically laminated, ternary transition metal borides, *Int. Mater. Rev.* 65 (4) (2020) 226–255.
- [15] M. Ade, H. Hillebrecht, Ternary borides Cr_2AlB_2 , Cr_3AlB_4 , and Cr_4AlB_6 : the first members of the series $(\text{CrB}_2)_n$ CrAl with $n = 1, 2, 3$ and a unifying concept for ternary borides as MAB-phases, *Inorg. Chem.* 54 (13) (2015) 6122–6135.
- [16] A.J. Mannix, X.-F. Zhou, B. Kiraly, J.D. Wood, D. Alducin, B.D. Myers, X. Liu, B. L. Fisher, U. Santiago, J.R. Guest, Synthesis of borophenes: anisotropic, two-dimensional boron polymorphs, *Science* 350 (6267) (2015) 1513–1516.
- [17] M.W. Barsoum, T. El-Raghy, Synthesis and characterization of a remarkable ceramic: Ti_3SiC_2 , *J. Am. Ceram. Soc.* 79 (7) (1996) 1953–1956.
- [18] W. Jeitschko, H. Nowotny, Die kristallstruktur von Ti_3SiC_2 —ein neuer komplexcarbidge-typ, *Monatsh. Chem.-Chem. Monh.* 98 (2) (1967) 329–337.
- [19] W. Jeitschko, H. Nowotny, F. Benesovsky, Carbides of formula T_2MC , *J. Less Common Metals* 7 (2) (1964) 133–138.
- [20] S. Geller, R. Grant, U. Gonser, Crystal chemistry and magnetic structures of substituted $\text{Ca}_2[\text{Fe}(\text{Fe})\text{O}_5]$, *Prog. Solid State Chem.* 5 (1971) 1–26.
- [21] B.U. Haq, S.-H. Kim, S. Tahir, R. Ahmed, S. AlFaify, K. Alam, A.R. Chaudhry, Theoretical investigations of O- and F-surface functionalization of MXenes based on Cr_2M (M = C, N), *Mater. Sci. Semicond. Process.* 168 (2023), 107837.
- [22] M.M.A. Bakhtiar Ul Haq, I.B. Khadka, R. Ahmed, S. AlFaify, Faheem K. Butt, Zulfiqar Ali Shah, Se-Hun Kim, First-principles study of the physical properties of Ti_2SnX (X = C, N) based 211 -MAX phases, *Chem. Phys.* 568 (2023), 111850.
- [23] S. Saad Essaoud, A.S. Jbara, Electronic-structural, thermo-electric, and thermo-mechanical properties of M_2AC and M_2AB (M = Nb or Mo, A = Al or Ga) compounds, *Indian J. Phys.* 97 (1) (2023) 105–114.
- [24] W. Zhou, L. Liu, P. Wu, First-principles study of structural, thermodynamic, elastic, and magnetic properties of Cr_2 2GeC under pressure and temperature, *J. Appl. Phys.* 106 (3) (2009), 033501.
- [25] A.S. Ingason, A. Mockute, M. Dahlqvist, F. Magnus, S. Olafsson, U.B. Arnalds, B. Alling, I.A. Abrikosov, B. Hjörvarsson, P.Å. Persson, Magnetic self-organized atomic laminate from first principles and thin film synthesis, *Phys. Rev. Lett.* 110 (19) (2013), 195502.
- [26] M. Dahlqvist, B. Alling, I. Abrikosov, J. Rosén, Magnetic nanoscale laminates with tunable exchange coupling from first principles, *Phys. Rev. B* 84 (22) (2011), 220403.
- [27] J. Wang, Y. Zhou, Dependence of elastic stiffness on electronic band structure of nanolaminate M_2AlC (M = Ti, V, Nb, and Cr) ceramics, *Phys. Rev. B* 69 (21) (2004), 214111.
- [28] J. Hettinger, S. Lofland, P. Finkel, T. Meehan, J. Palma, K. Harrell, S. Gupta, A. Ganguly, T. El-Raghy, M. Barsoum, Electrical transport, thermal transport, and elastic properties of M_2AlC (M = Ti, Cr, Nb, and V), *Phys. Rev. B* 72 (11) (2005), 115120.
- [29] K. Schwarz, P. Blaha, Solid state calculations using WIEN2k, *Comput. Mater. Sci.* 28 (2) (2003) 259–273.
- [30] J.P. Perdew, K. Burke, M. Ernzerhof, Generalized gradient approximation made simple, *Phys. Rev. Lett.* 77 (18) (1996) 3865.
- [31] B. Ul Haq, S. AlFaify, A. Laref, Exploring novel flat-band polymorphs of single-layered germanium sulfide for high-efficiency thermoelectric applications, *J. Phys. Chem. C* 123 (30) (2019) 18124–18131.
- [32] S.U. Rehman, F.K. Butt, F. Hayat, B.U. Haq, Z. Tariq, F. Aleem, C. Li, An insight into a novel cubic phase SnSe for prospective applications in optoelectronics and clean energy devices, *J. Alloys Compd.* 733 (2018) 22–32.
- [33] Q. Mahmood, M. Yaseen, B.U. Haq, A. Laref, A. Nazir, The study of mechanical and thermoelectric behavior of MgXO_3 (X = Si, Ge, Sn) for energy applications by DFT, *Chem. Phys.* 524 (2019) 106–112.
- [34] M.S. Khan, T. Alshahrani, B.U. Haq, S. Azam, G. Khan, H. Alrobei, Z. Abbas, M. Predota, M.A. Khan, M. Benaadad, Investigation of structural, electronic and optical properties of potassium and lithium based ternary Selenoindate: using first principles approach, *J. Solid State Chem.* 293 (2021), 121778.
- [35] B.U. Haq, M.B. Kanoun, R. Ahmed, M. Bououdina, S. Goumri-Said, Hybrid functional calculations of potential hydrogen storage material: complex dimagnesium iron hydride, *Int. J. Hydrogen Energy* 39 (18) (2014) 9709–9717.
- [36] B.U. Haq, S. AlFaify, A. Laref, R. Ahmed, F.K. Butt, A.R. Chaudhry, S.U. Rehman, Q. Mahmood, Optoelectronic properties of new direct bandgap polymorphs of single-layered Germanium sulfide, *Ceram. Int.* 45 (14) (2019) 18073–18078.
- [37] B.U. Haq, T. Alshahrani, R. Ahmed, Q. Mahmood, D. Hoat, S. Tahir, Investigations of thermoelectric properties of ZnO monolayers from the first-principles approach, *Phys. E Low-dimens. Syst. Nanostruct.* 126 (2021), 114444.
- [38] B.U. Haq, R. Ahmed, A. Shaari, N. Ali, Y. Al-Douri, A. Reshak, Comparative study of Fe doped ZnO based diluted and condensed magnetic semiconductors in wurtzite and zinc-blende structures by first-principles calculations, *Mater. Sci. Semicond. Process.* 43 (2016) 123–128.
- [39] B.U. Haq, R. Ahmed, A. Shaari, A. Afaq, B. Tahir, R. Khenata, First-principles investigations of Mn doped zinc-blende ZnO based magnetic semiconductors: materials for spintronic applications, *Mater. Sci. Semicond. Process.* 29 (2015) 256–261.
- [40] B.U. Haq, R. Ahmed, J.Y. Rhee, A. Shaari, S. AlFaify, M. Ahmed, Composition-induced influence on the electronic band structure, optical and thermoelectric coefficients of the highly mismatched GaSnB alloy over the entire range: a DFT analysis, *J. Alloys Compd.* 693 (2017) 1020–1027.
- [41] B.U. Haq, R. Ahmed, M. Mohamad, A. Shaari, J. Rhee, S. AlFaify, M.B. Kanoun, S. Goumri-Said, Engineering of highly mismatched alloy with semiconductor and semi-metallic substituent's for photovoltaic applications, *Curr. Appl. Phys.* 17 (2) (2017) 162–168.
- [42] T. Ghrib, A. Rached, E. Algrafy, I.A. Al-naum, H. Albalawi, M. Ashiq, B.U. Haq, Q. Mahmood, A new lead free double perovskites $\text{K}_2\text{Ti}(\text{Cl}/\text{Br})_6$: a promising materials for optoelectronic and transport properties: probed by DFT, *Mater. Chem. Phys.* 264 (2021), 124435.
- [43] S. Al-Qaisi, M.A. Ali, T.A. Alrebdi, T.V. Vu, M. Morsi, B.U. Haq, R. Ahmed, Q. Mahmood, S.A. Tahir, First-principles investigations of Ba_2NaIO_6 double perovskite semiconductor: material for low-cost energy technologies, *Mater. Chem. Phys.* 275 (2022), 125237.
- [44] R. Ahmed, N.S. Masuri, B.U. Haq, A. Shaari, S. AlFaify, F.K. Butt, M.N. Muhamad, M. Ahmed, S.A. Tahir, Investigations of electronic and thermoelectric properties of half-Heusler alloys XMgN (X = Li, Na, K) by first-principles calculations, *Mater. Des.* 136 (2017) 196–203.
- [45] C. Zuo, B. Chen, C. Zhong, J. Zhao, The structural, electronic, elastic and thermodynamic properties of V_2AX (A = B, Al, Ga, in and Ti; X = C and N): a DFT calculation, *Int. J. Mod. Phys. B* 33 (30) (2019), 1950359.
- [46] A. Bouhemadou, Calculated structural and elastic properties of M_2InC (M = Sc, Ti, V, Zr, Nb, Hf, Ta), *Mod. Phys. Lett. B* 22 (22) (2008) 2063–2076.
- [47] I. Shein, A. Ivanovskii, Graphene-like titanium carbides and nitrides $\text{Ti}_n + 1\text{C}_n$, $\text{Ti}_n + 1\text{N}_n$ ($n = 1, 2$, and 3) from de-intercalated MAX phases: first-principles probing of their structural, electronic properties and relative stability, *Comput. Mater. Sci.* 65 (2012) 104–114.
- [48] S. Aydin, 211 -MAX borides: the stable boron-substituted 211 -MAX compounds by first-principles, *Mater. Today Commun.* 25 (2020), 101689.
- [49] Y. Bai, X. He, M. Li, Y. Sun, C. Zhu, Y. Li, Ab initio study of the bonding and elastic properties of Ti_2CdC , *Solid State Sci.* 12 (1) (2010) 144–147.